Journal of Power Sources 197 (2012) 305–309

Contents lists available at SciVerse ScienceDirect

Journal of Power Sources

journal homepage: www.elsevier.com/locate/jpowsour

Short communication

Hollow Fe_3O_4/C spheres as superior lithium storage materials

Qiumei Zhang [a,b], Zhicong Shi [a,b,*], Yuanfu Deng [b,c,**], Jun Zheng [b], Guichang Liu [a], Guohua Chen [a,b,d,**]

[a] State Key Laboratory of Fine Chemicals, School of Chemical Engineering, Dalian University of Technology, Dalian 116023, China
[b] Center for Green Products and Processing Technologies, Guangzhou HKUST Fok Ying Tung Research Institute, Guangzhou 511458, China
[c] Department of Chemistry, School of Chemistry and Chemical Engineering, South China University of Technology, Guangzhou 510640, China
[d] Department of Chemical and Biomolecular Engineering, The Hong Kong University of Science and Technology, Hong Kong, China

ARTICLE INFO

Article history:
Received 30 July 2011
Received in revised form 8 September 2011
Accepted 12 September 2011
Available online 16 September 2011

Keywords:
Lithium ion battery
Anode material
Spinel iron oxide
Hollow sphere
High capacity

ABSTRACT

Unique hollow Fe_3O_4/C spheres are prepared by a simple one-pot solvothermal method, with spinel structure and 750 nm in diameter identified by X-ray diffraction (XRD), scanning electron microscopy (SEM) and transmission electron microscopy (TEM) techniques. The hollow Fe_3O_4/C spheres exhibit excellent cycling and rate performance as anode material for lithium ion batteries, delivering reversible specific capacities of 984 mAh g^{-1} even after 70 cycles at 0.2 C, 620 mAh g^{-1} at 2 C, and 460 mAh g^{-1} at 5 C, respectively. Lithium insertion mechanisms are also proposed in terms of the *ex situ* XRD analysis of the electrodes after discharged and charged to certain voltages together with cyclic voltammetry (CV) and voltage profile.

Crown Copyright © 2011 Published by Elsevier B.V. All rights reserved.

1. Introduction

In recent years, nano transition metal oxides such as titanium oxides, manganese oxides, and iron oxides have been investigated as anode materials for lithium ion batteries (LIBs) [1–3]. Fe_3O_4 is an interesting one due to its high theoretical specific capacity, low cost and environmental benignity [4–10]. However, it suffers much from its low rate capabilities, big difference between charging voltage and discharging one, and poor capacity retention arising from kinetic limitations, agglomerations and large volume expansion occurring during cycling. Carbon coating [11–13] and porous structure [14] have been demonstrated as effective ways to overcome the above-mentioned shortage in other transition metal oxides. But to our knowledge, there is no report on combined use of these two strategies for Fe_3O_4.

Herein, nearly mono-dispersed hollow Fe_3O_4/C spheres were successfully self-assembled with small particles by a facile and energy-saving solvothermal route with superior lithium storage performance as anode materials for LIBs. In addition, possible lithium insertion mechanisms are also proposed based on the *ex situ* XRD analysis of the electrodes after discharged and charged to selective voltage.

2. Experimental

Uniform hollow spherical Fe_3O_4/C composites were synthesized by solvothermal treatment of $FeCl_3 \cdot 6H_2O$ (5 mmol), urea (45 mmol) and PEG-2000 (1.00 g) in ethylene glycol (EG, 35 mL) solution at 200 °C for 48 h, with the following cooling, centrifugation, and drying at vacuum oven at 100 °C for 12 h.

The crystalline structure and morphology were characterized by XRD (Bruker D8 ADVANCE, Cu Kα radiation, λ = 1.5406 nm), SEM (JEOL 6300F) and HRTEM (PHILIPS TECNAI F30). The carbon content was 2.3 wt% confirmed by elemental analysis (Elementar vario EL III). Composite electrodes consisting of 50 wt% Fe_3O_4/C, 30 wt% acetylene black and 20 wt% polyvinylidene fluoride (PVdF) were made on copper foil. The specific capacities were calculated based on the mass of Fe_3O_4/C. Coin-type half-cells (CR2025) were assembled in an argon-filled glove box (MBRAUN LAB MASTER130) with 1.0 mol L^{-1} of $LiPF_6$ solution in ethylene carbonate/ethylene methyl carbonate/dimethyl carbonate (EC:EMC:DMC = 1:1:1, v/v/v) as the electrolyte and Celgard 2400 as the separator, and were tested in the voltage range between 3.00 and 0.01 V on battery test station (NEWARE CT-3008W). The cyclic voltammetric (CV) measurement was performed on an Electrochemical Workstation (AUTOLAB PGSTAT 101) at a scan rate of 0.1 mV s^{-1} in the range of 3.00–0.01 V vs. Li/Li^+. The *ex situ* XRD experiments were investigated using the Bruker D8 ADVANCE powder diffractometer with Cu Kα radiation at 40 kV and 40 mA in steps of 0.02. At the end of discharge in certain cycles, the AC impedance spectra of the cells were measured on an electrochemical workstation (ZAHNER ZENNIUM) in

* Corresponding author. Tel.: +86 20 34685679; fax: +86 20 34685679.
** Corresponding authors.
E-mail addresses: zhicong@ust.hk, zcshi@dlut.edu.cn (Z. Shi), chyfdeng@scut.edu.cn (Y. Deng), kechengh@ust.hk (G. Chen).

0378-7753/$ – see front matter. Crown Copyright © 2011 Published by Elsevier B.V. All rights reserved.
doi:10.1016/j.jpowsour.2011.09.029

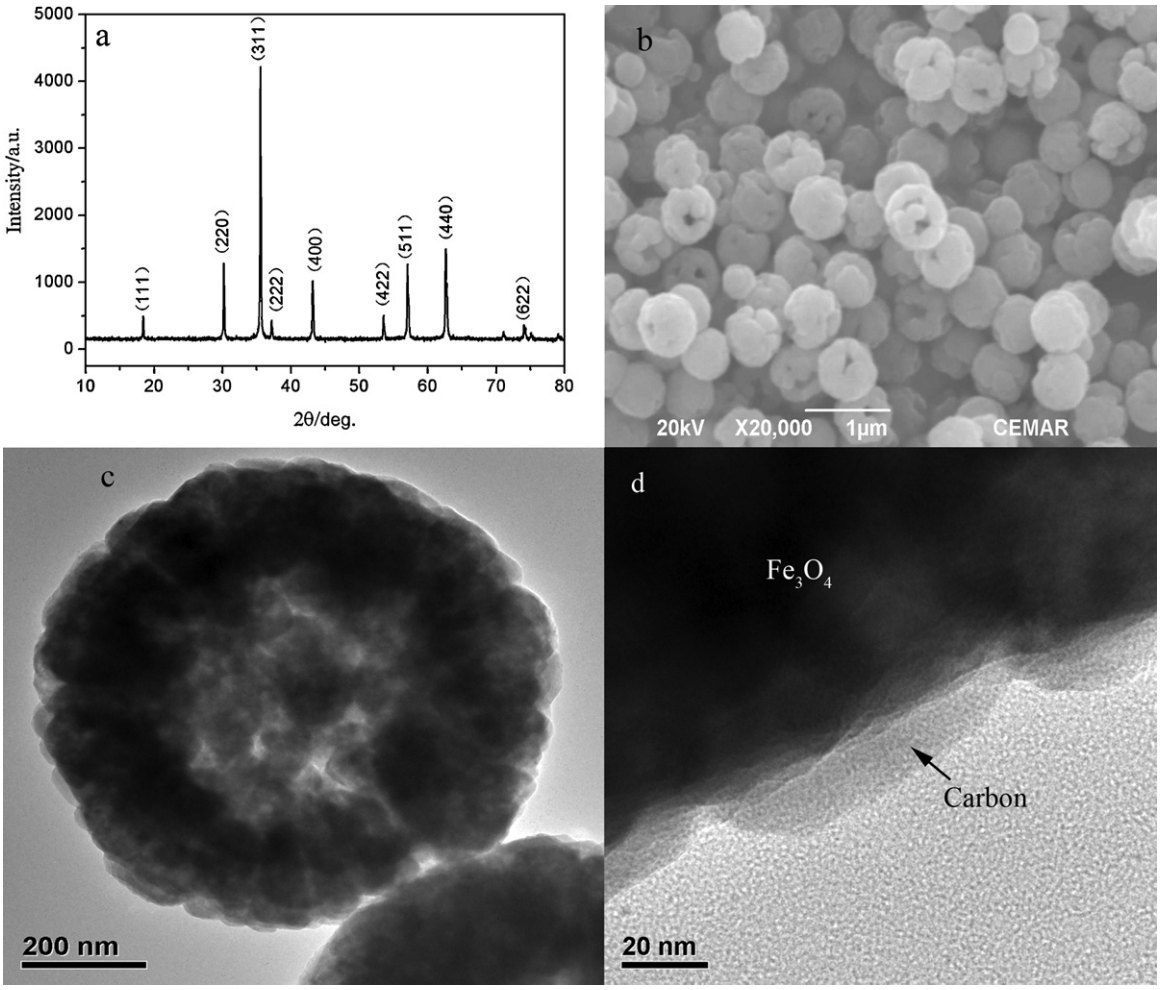

Fig. 1. XRD pattern (a), SEM (b), TEM (c), and HRTEM (d) images of Fe_3O_4/C synthesized via solvothermal method at 200 °C for 48 h.

the frequency range from 10^5 to 10^{-2} Hz with the excitation voltage of 10 mV.

3. Results and discussion

The structure and composition of the as-synthesized samples were confirmed by XRD and elemental analysis (EA). All the peaks in XRD pattern are indexed to be from the cubic phase of Fe_3O_4 (JCPDS Card No. 19-0629) (Fig. 1a). The EA result shows that the carbon content of this sample is 2.3 wt%. However no diffraction peak corresponding to graphitic carbon was observed in the XRD pattern, revealing that the carbon was amorphous. The chemical composition of 97.7 wt% Fe_3O_4 and 2.3 wt% carbon leads to a theoretical specific capacity of 911.3 mAh g^{-1} for the Fe_3O_4/C spheres when being used as anode material for LIBs.

Unique hollow Fe_3O_4/C spheres can be identified by the SEM, TEM, and HRTEM images. The nano-particles stacked products are hollow spherical with opening on the surface for electrolyte passing through and an average diameter of 750 nm (Fig. 1b). The spheres wall is 200 nm in thickness (Fig. 1c) with the carbon film of 15 nm coated on the Fe_3O_4 lattice (Fig. 1d). We also performed Raman analysis of the samples and proved the existence of the carbon. Therefore, EA, HRTEM, and Raman analysis clearly confirmed the successful coating of carbon on the surface of the hollow Fe_3O_4/C spheres by one-pot solvothermal route. In this system, the presence of EG played three important roles as high-boiling-point solvent, reducing agent, and carbon precursor for the preparation of hollow Fe_3O_4/C spheres [15,16].

The electrochemical properties of the hollow Fe_3O_4/C spheres as anode material for LIBs were investigated. The voltage profile of Fe_3O_4/C between 3.00 and 0.01 V in the first discharge shows a short voltage plateau at 0.85 V and a long one at 0.80 V (Fig. 2a). The first discharge curve shows a continuous voltage decrease from the open circuit voltage to 0.85 V with 0.6 mol Li^+ intercalating during a single-phase reaction, which can be ascribed to the formation of $Li_xFe_3O_4$ [9]. The following Li^+ insertion results in a voltage plateau at 0.85 V, which extends up to a consumption of 1.0 mol Li^+ to form $LiFe_3O_4$ phase. At 0.80 V, phase transformation reaction happened with the incomplete reduction of Fe^{3+}/Fe^{2+} to Fe^{2+}/Fe^0 and the formation of amorphous Li_2O. As the voltage decreases gradually down to 0.01 V, an whole initial specific capacity of 1259 mAh g^{-1} attributed to further reduction of Fe^{2+} to Fe^0can be achieved, which is higher than the theoretical one of Fe_3O_4. The extra capacity over the theoretical one arises from the decomposition of the solvent in the electrolyte to form a solid electrolyte interphase (SEI) and lithium ions insertion into acetylene black [15,17–19]. This first discharge profile of the Fe_3O_4/C is similar to the reported ones [4–8], except for a small 0.85 V plateau. The first charge curve shows no voltage plateau with an overall specific capacity of 864 mAh g^{-1}, corresponding to the reversible oxidation of Fe^0 to Fe^{2+} and Fe^{3+}. The following voltage profiles were changed into slopes during Li^+ insertion/deinsertion process, which well agrees with the two cathodic/anodic peak pairs in the CV profiles (Fig. 2c). The reversible specific capacity of Fe_3O_4/C gradually increases to 998 mAh g^{-1} until the 12th cycle corresponding to the activation process associated with the partial crystallinity degradation of the

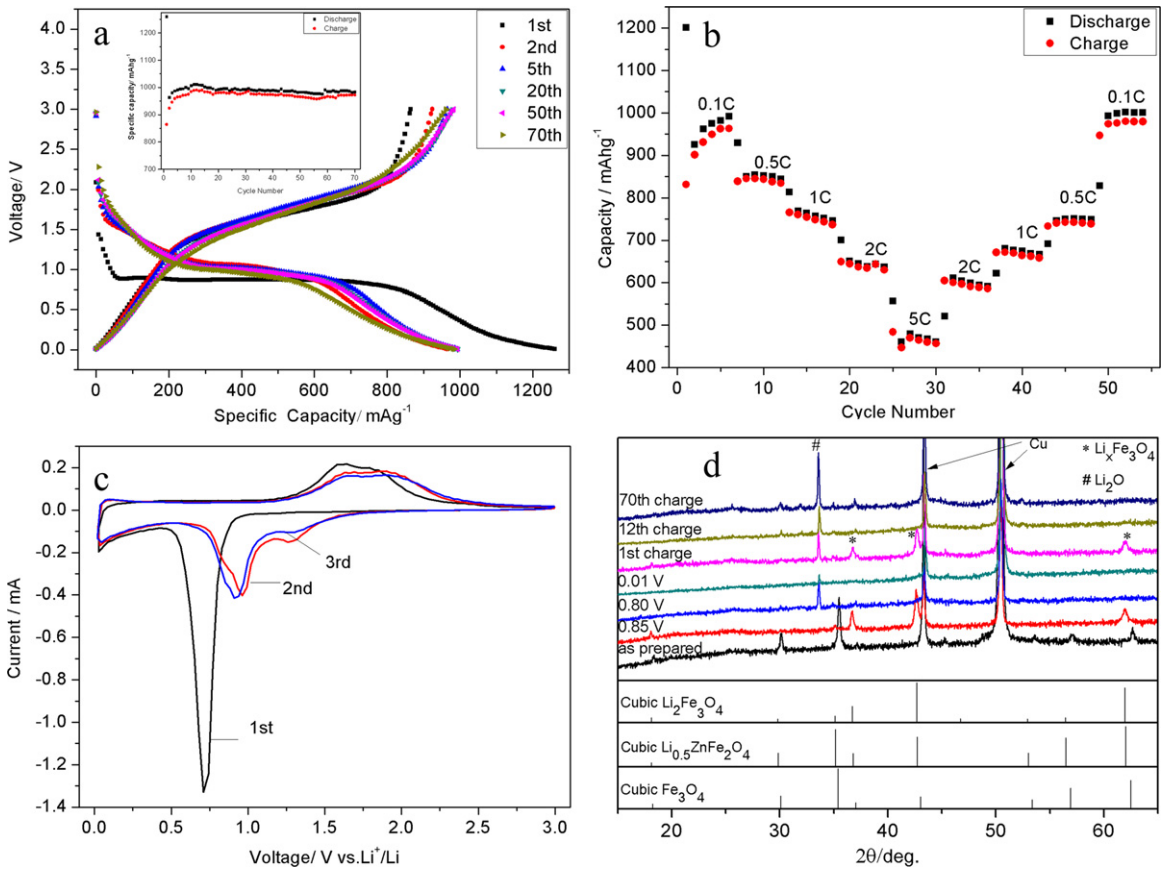

Fig. 2. Charge–discharge curves (a), cycling performance (a, inset) at 0.2 C, rate performance (b), and cyclic voltammograms (c) at a scan rate of 0.1 mV s^{-1} of the Fe_3O_4/C spheres vs. Li^+/Li. *Ex situ* XRD patterns (d) of Fe_3O_4/C discharged and charged to certain voltages (vs. Li^+/Li) during the initial and following cycles.

Fe_3O_4/C spheres during initial cycling [20] (Fig. 2a, inset). Then the specific capacity decays very slowly and almost maintains at 984 mAh g^{-1} during 70 cycles at 0.2 C, demonstrating high capacity retention capability of unique Fe_3O_4/C spheres.

Besides the improved cycling performance, the hollow Fe_3O_4/C spheres also display very good rate performance (Fig. 2b). A reversible specific capacity of 620 mAh g^{-1} at 2 C and 460 mAh g^{-1} at 5 C can be obtained, far higher than that of commercial graphite. The capacities of the Fe_3O_4/C were higher than or comparable to reported carbon-coated or graphene-wrapped Fe_3O_4 [4,6–9]. After charging/discharging at high rates, the specific capacity can be recovered to 1000 mAh g^{-1} at 0.1 C. The high capacities observed at high rates imply that this kind of Fe_3O_4 hollow spheres could be promising anode materials for power LIBs. The enhanced rate and retention capability of Fe_3O_4 material are attributed to the unique hollow spherical structure and evenly dispersed carbon, which not only favor a fast kinetic property with facilitating the electron transportation and the Li^+ insertion/deinsertion but also less volume expansion during cycling.

The CV profiles for the initial three cycles are shown in Fig. 2c. In the first cycle, the sole peak at 0.70 V in the cathodic process could be attributed to the reduction of Fe^{3+} and Fe^{2+} to Fe^0 [9]. While two peaks at 1.60 and 1.75 V were recorded in the reverse process, corresponding to the reversible oxidation of Fe^0 to Fe^{2+} and Fe^{3+} [4–8]. Caused by the polarization of the Fe_3O_4/C in the first cycle, both cathodic and anodic peaks are positively shifted in the subsequent cycles [10]. A new peak at 1.30 V in the cathodic process was observed, which may relate to the reaction of Fe^{3+} and Fe^{2+} to Fe^0 occurs in two steps that involve intermediate phases. During the anodic process, both the peak current and the integrated area of the anodic peak are almost unchanged, indicating excellent capacity retention during the following charging process.

Fe_3O_4 as anode materials for LIBs has been widely investigated in previous literatures, but the exact lithium insertion mechanism is still controversial. We herein propose the lithium insertion mechanisms in terms of the *ex situ* XRD analysis of Fe_3O_4/C after discharged or charged to certain voltages (Fig. 2d) together with charge/discharge curves (Fig. 2b). When the Fe_3O_4/Li cell was first discharged to 0.85 V, the diffraction peaks of Fe_3O_4 disappeared, accompanied by some new broad peaks ascribed to $Li_xFe_3O_4$ ($0 < x < 2$) [9,21,22]. Therefore, a two phase reaction was being conducted at 0.85 V. A new peak at $2\theta = 33.5^\circ$ in the XRD pattern corresponding Li_2O (PDF-12-0254) was observed when the cell was discharged to 0.80 V, which existed until the deep discharge limit of 0.01 V. However, no obvious XRD peaks corresponding to metallic Fe could be found when the cell discharged to 0.01 V due to diffraction peaks broadening, which can be attributed to the nanoparticle nature of the electrochemically formed species [23]. When the cell was recharged to 3.00 V at the first cycle, diffraction peaks corresponding to $Li_xFe_3O_4$ appeared again with that of Li_2O resulting from the irreversible Li^+. However, this $Li_xFe_3O_4$ interphase is observed for the first time in charge process, which has not been mentioned in the previous literatures [9,21,22]. The $Li_xFe_3O_4$ phase faded away at the 12th cycle, which agreed well with the fact that the material conducted an activation process during the first 12 cycles (Fig. 2a). However, new peaks corresponding to Fe_3O_4 began to appear in the 12th charge state and this peak became stronger in the 70th charge state, which could in turn prove its excellent cyclability after 12th cycle (Fig. 2a inset).

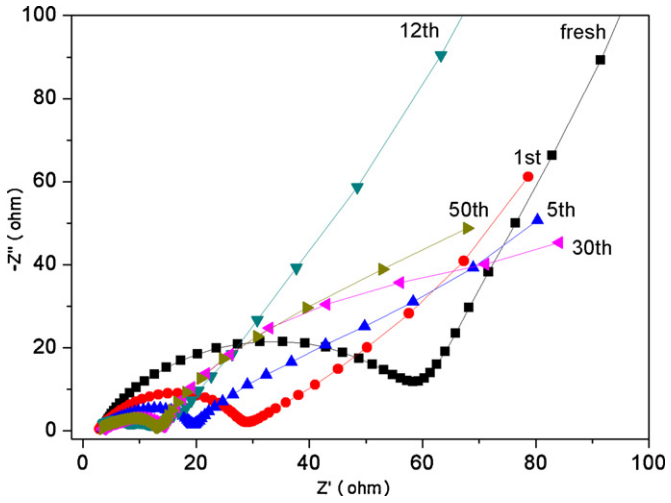

Fig. 3. AC impedance (Nyquist plots) of Li/Fe_3O_4 cells performed in the frequency range between 10^5 and 10^{-2} Hz at the open-circuit voltage of fresh or full discharged state after certain cycles.

Based on the discharge/charge curve and *ex situ* XRD analysis, the possible lithium storage mechanism of the Fe_3O_4/C spheres is proposed. A total of 8 mol Li^+ per formula participate in the initial discharge process, x mol of Li^+ ($0 < x < 2$) ions for the intercalation reaction [Eq. (1)] and $(8-x)$ Li^+ ions for the conversion reaction Eq. (2). A total specific capacity of 924 mAh g^{-1} can be obtained from the two reactions. The extra capacity of 333 mAh g^{-1} can be attributed to the decomposition of the solvent in the electrolyte to form a gel-like film and the formation of a solid electrolyte interphase (SEI)/irreversible Li_2O in the first cycle [15,17,18,20]. The first charge up to 3.00 V recovers a capacity of 864 mAh g^{-1}, which matches well with Eq. (3), however the 12th and 70th charge specific capacities are 982 and 978 mAh g^{-1} respectively, which are all higher than the consume capacity of Eqs. (3) and (4). This capacity rise phenomenon has been widely demonstrated in the transition metal oxide electrodes, which is attributed to the formation of a gel-like organic layer on the surface of hollow spheres and hollow nanoparticles. These hollow structures may bring more active sites, such as mesopores, defects and vacancies in the walls of hollow nanoparticles, for lithium ion storage, hence to improve the specific capacity [5,21,24,25].

$$Fe_3O_4 + xLi^+ + xe^- \rightarrow Li_xFe_3O_4 \quad (1)$$

$$Li_xFe_3O_4 + (8-x)Li^+ + (8-x)e^- \rightarrow 4Li_2O + 3Fe \quad (2)$$

$$3Fe + 4Li_2O \rightarrow Li_xFe_3O_4 + (8-x)Li^+ + (8-x)e^- \quad (3)$$

$$Li_xFe_3O_4 + xe^- \rightarrow xLi^+Fe_3O_4 + xe^- \quad (4)$$

To further understand the superior electrochemical performance of spherical Fe_3O_4/C as anode material, the AC impedance of Fe_3O_4/Li cells in the fresh and discharged states after certain cycles (1st, 5th, 12th, 30th and 50th) are performed (Fig. 3). The Nyquist plots are similar to each other in the shape, with a depressed semicircle in the high and medium frequency ranges and a straight line in the low frequency. For the fresh cell, the depressed semicircle in the high and medium frequency region is attributed to the impedance containing charge transfer resistance (R_{ct}) and double layer capacitance (C_{dl}). After discharge process, a surface layer normally named solid electrolyte interface (SEI) will be formed on the surface of anode material. But it is interesting that we cannot find 2 separated semicircles in the Nyquist plots to identify 2 electrochemical processes through double layer and SEI, which is totally different from that in the previous report on Fe_3O_4 with submicron spheroids [9], nanorods [19], and nanofibers [25] structures. During cycling, the resistances calculated from the depressed semicircles decrease gradually from 60 Ω in the 1st discharge state to 11 Ω in the 12th discharge state as evident from Fig. 3. Then the resistance again slowly rises to 13 Ω in the 30th discharge state, and remains almost unchanged after the 30th cycle. This impedance evolution can well match the excellent electrochemical performance with the reversible specific capacity gradually increasing from 864 mAh g^{-1} at the 1st cycle to 998 mAh g^{-1} at the 12th cycle, and then decrease a little to 984 mAh g^{-1} during the latter 40 cycles (Fig. 2a, inset).

4. Conclusions

In summary, hollow Fe_3O_4/C spheres have been synthesized via a one-pot solvothermal method using low cost starting materials. The synthesized hollow spheres were used for the first time as anode materials for LIBs. A large initial discharge specific capacity of 1259 mAh g^{-1} was obtained with 984 mAh g^{-1} retained after 70 cycles at 0.2 C rate. This material exhibited good rate performance and cycling stability, which could be attributed to the enhanced kinetic properties of the hollow spherical structure and improved conductivity via the even dispersed carbon in the composite material. Lithium insertion mechanisms are also proposed in terms of the *ex situ* XRD analysis of the electrodes in this work. These finding motivates us to design novel hollow spherical structure electrode materials for LIBs to be applied in electrical vehicles and energy storage area.

Acknowledgements

This work is supported by the Fundamental Research Funds for the Central Universities (DUT10JN06, SCUT2009ZM0313), the Specialized Research Fund for the Doctoral Program of Higher Education of China (20090041120020), the GDSTC IER Innovative Platform Funds of China (2010B091000004), the Fok Ying Tung Foundation (NRC07/08.EG01) and the NNFSC (20801020, 21176045).

References

[1] X.W. Lou, L.A. Archer, Z.C. Yang, Adv. Mater. 20 (2008) 3987–4019.
[2] Y.G. Wang, H.Q. Li, P. He, E. Hosono, H.S. Zhou, Nanoscale 2 (2010) 1294–1305.
[3] P. Poizot, S. Laruelle, S. Grugeon, L. Dupont, J.M. Tarascon, Nature 407 (2000) 496–499.
[4] W.M. Zhang, X.L. Wu, J.S. Hu, Y.G. Guo, L.J. Wan, Adv. Funct. Mater. 18 (2008) 3941–3946.
[5] J.S. Zhou, H.H. Song, X.H. Chen, L.J. Zhi, S.B. Yang, J.P. Huo, W.T. Yang, Chem. Mater. 21 (2009) 2935–2940.
[6] Z.M. Cui, L.Y. Jiang, W.G. Song, Y.G. Guo, Chem. Mater. 21 (2009) 1162–1166.
[7] G.M. Zhou, D.W. Wang, F. Li, L.L. Zhang, N. Li, Z.S. Wu, L. Wen, G.Q. Lu, H.M. Cheng, Chem. Mater. 22 (2010) 5306–5313.
[8] M. Zhang, D.N. Lei, X.M. Yin, L.B. Chen, Q.H. Li, Y.G. Wang, T.H. Wang, J. Mater. Chem. 22 (2010) 5538–5543.
[9] S.Q. Wang, J.Y. Zhang, C.H. Chen, J. Power Sources 195 (2010) 5379–5381.
[10] J.Z. Wang, C. Zhong, D. Wexler, N.H. Idris, Z.X. Wang, L.Q. Chen, H.K. Liu, Chem. A. Eur. J. 17 (2011) 661–667.
[11] Y.S. Hu, R. Demir-Cakan, M.M. Titirici, J.O. Muller, R. Schlogl, M. Antonietti, J. Maier, Angew. Chem. Int. Ed. 47 (2008) 1645–1649.
[12] X.W. Lou, J.S. Chen, P. Chen, L.A. Archer, Chem. Mater. 21 (2009) 2868–2874.
[13] H.L. Wang, L.F. Cui, Y. Yang, H.S. Casalongue, J.T. Robinson, Y.Y. Liang, Y. Cui, H.J. Dai, J. Am. Chem. Soc. 130 (2010) 13978–13980.
[14] S.J. Ding, J.S. Chen, G.G. Qi, X.N. Duan, Z.Y. Wang, E.P. Giannelis, L.A. Archer, X.W. Lou, J. Am. Chem. Soc. 133 (2011) 21–23.
[15] Y.F. Deng, Q.M. Zhang, S.D. Tang, L.T. Zhang, S.N. Deng, Z.C. Shi, G.H. Chen, Chem. Commun. 47 (2011) 6828–6830.
[16] S.H. Liu, R.M. Xing, F. Lu, R.K. Rana, J.J. Zhu, J. Phys. Chem. C 113 (2009) 21042–21047.
[17] S. Laruelle, S. Grugeon, P. Poizot, M. Dolle, L. Dupont, J.M. Tarascon, J. Electrochem. Soc. 149 (2002) A627–A634.
[18] Y. Wang, F.B. Su, J.Y. Lee, X.S. Zhao, Chem. Mater. 5 (2006) 1347–1353.
[19] H. Liu, G.X. Wang, J.Z. Wang, D. Wexler, Electrochem. Commun. 10 (2008) 1879–1882.

[20] L.C. Yang, Q.S. Gao, Y.H. Zhang, Y. Tang, Y.P. Wu, Electrochem. Commun. 10 (2008) 118–122.
[21] S.L. Jin, H.G. Deng, D.H. Long, X.J. Liu, L. Zhan, X.Y. Liang, W.M. Qiao, L.C. Ling, J. Power Sources 196 (2011) 3887–3893.
[22] Y. He, L. Huang, J.S. Cai, X.M. Zheng, S.G. Sun, Electrochim. Acta 55 (2010) 1140–1144.
[23] Y.F. Deng, S.D. Tang, Q.M. Zhang, Z.C. Shi, L.T. Zhang, S.Z. Zhan, G.H. Chen, J. Mater. Chem. 21 (2011) 11987–11995.
[24] P.C. Wang, H.P. Ding, T. Bark, C.H. Chen, Electrochim. Acta 52 (2007) 6650–6655.
[25] L. Wang, Y. Yu, P.C. Chen, D.W. Zhang, C.H. Chen, J. Power Sources 183 (2008) 717–723.